Eur. Phys. J. D **7**, 31–38 (1999)

**THE EUROPEAN PHYSICAL JOURNAL D**

EDP Sciences


# Neutralization of specularly reflecting $H^+$ ions on a clean (001) surface of SnTe

Y. Susuki[a]

Department of Physics, Osaka Kyoiku University, Kashiwara, Osaka 582-8582, Japan

Received: 23 October 1998

**Abstract.** Neutral fractions of specularly reflected beams have been measured for the glancing-angle incidence of (0.2–0.5) MeV $H^+$ ions on a clean (001) surface of SnTe. The measured fractions have been compared with the results calculated by a classical model for charge exchanges and by a model based on the first-order perturbation theory. The experimental and calculated results have differed greatly. The disagreements are attributed to collisions with valence electrons on the surface. The electron capture cross-sections of (0.2–0.5) MeV $H^+$ ions for valence electrons have been derived, based on the measured neutral fraction and distribution of valence electrons for jellium background positive charges, and are found to be about ten times larger than those for the outermost electrons of Sn and Te atoms calculated by the classical model.

**PACS.** 79.20.Rf Atomic, molecular, and ion beam impact and interactions with surfaces – 34.70.+e Charge transfer – 34.50.Bw Energy loss and stopping power

## 1 Introduction

For many years, investigations of the charge exchange of energetic ions on atoms or molecules have been interesting in atomic physics, plasma physics and ion implantation technology [1–3]. Theoretical treatments of atomic collision processes have also been used to investigate the charge exchange of ions in solids and on solid surfaces [3]. When isolated atoms form a solid, the energy states and distributions of the outermost electrons are modified, while the changes of those of the inner-shell electrons are small. In the electron capture of the energetic ions ($v > 3v_0$, where $v$ is the ion velocity and $v_0$ is the Bohr velocity) from a target atom, the contribution of inner-shell electrons of the atom is important, but that of the outermost electrons is negligibly small. Thus the charge exchange process in solids can be described by a model based on the atomic collision process regardless of the changes in the states of the valence electrons arising from the formation of the solid.

At the glancing-angle incidence of MeV ions on the surface of a single crystal, the ions interact with the surface in a vacuum along trajectories near parallel to the surface [4]. The closest approaches of the ions to the surface atomic plane can be as small as 1 Å at the angle of incidence of sub MeV protons less than 5 mrad. Thus studies of the role of the valence electrons on the surface in the charge exchange process are possible. The role may be important, because the density of the inner-shell electrons is negligible at distances from the surface larger than 1 Å [5–8].

In this paper, we report neutral fractions of specularly reflected beams measured for a glancing-angle incidence of (0.2–0.5) MeV $H^+$ ions on a clean (001) surface of SnTe. The measured fractions are compared with calculated results based on classical Bohr and Bohr-Lindhard models and those of the first-order perturbation theory. The electron capture cross-sections of (0.2–0.5) MeV $H^+$ ions for these electrons are derived from the measured neutral fractions by introducing a distribution of valence electrons for jellium background positive charges at the surface.

## 2 Experimental

The experimental setup is described elsewhere [9,10], and only relevant points are mentioned here.

A clean (001) surface of SnTe crystal was prepared by *in situ* evaporation of pure SnTe (99.999%) on a KCl (001) cleavage surface under a vacuum condition of $10^{-10}$ Torr. The (0.2–0.5) MeV/amu $H_2^+$ or $H_3^+$ ions were accelerated by the 4 MV Van de Graaff accelerator of Kyoto University. The molecular ions were dissociated in collisions with $N_2$ molecules in a collision cell. The $H^+$ fragment-ions were analyzed by a 90° magnet, collimated to obtain a maximal angular divergence of 0.1 mrad, and were scattered on the clean (001) surface of SnTe. The angle of incidence of the beam to the surface is denoted by $\theta_i$ and

[a] e-mail: susuki@cc.osaka-kyoiku.ac.jp

the angle of scattering measured from the incident beam direction in the scattering plane, which contains the surface normal and the incident beam direction, is denoted by $\theta_s$. The azimuthal angle of incidence was carefully adjusted to avoid the surface channeling of ions along the low-index crystal axes. The distributions of the yields of scattered $H^+$ ions on the angle of scattering $\theta_s$ peaked at the angle of specular reflection ($\theta_s = 2\theta_i$). Although the width of the distribution was influenced by the angle and energy of incidence, the typical FWHM was 5 mrad.

Neutral fractions of the scattered ions were measured by removing charged $H^+$ with an analyzing magnet placed downstream of the aperture, which defines the angle of scattering with an acceptance half-angle of 0.33 mrad. Ions were counted with a solid-state detector (SSD) whose energy resolution was 11.5 keV. The signals from the SSD were amplified and the amplified pulses were collected by a multichannel analyzer (ORTEC model 7100) which was controlled by a sequential pulse generator for a period of 9 s. The sequences to measure the total ions $H^+$ ($+H^0$) and neutral $H^0$ were then repeated. The time ratio of the measurements in the period, $\tau_0/\tau_+$, was 14.6, where $\tau_0$ is the measuring time for $H^0$ and $\tau_+$ is that for $H^+$ ($+H^0$). The time interval between the two measurements in each period was long enough to stabilize the magnetic field. The fraction of $H^-$ was less than $10^{-4}$ and was neglected in this work.

A pair of examples of the energy spectra of total $H^+$ ($+H^0$) and neutral $H^0$ are shown in Figure 1 at 0.2 MeV $H^+$ incidence. Since the neutral fraction is less than 1%, the energy spectrum of the total ions is considered to be that of the $H^+$ ions. It has been reported that ions reflected from the (001) surface of SnTe show an energy spectrum consisting of a small number of subpeaks, resulting from penetration through and reappearance from the topmost atomic layer of the surface [10,11]. However, the structure cannot be seen in Figure 1 because of the poor resolution of the solid-state detector. The oscillatory structure is smeared and appears as a low-energy tail of the spectra [12,13]. The ratio of ions reflected from the topmost atomic layer to the ions detected in the SSD can be checked by the incidence of MeV $He^+$ ions. More than 50% of the scattered He ions measured at the angle for specular reflection were reflected from the topmost atomic layer. The ratio for $H^+$ ions may be close to this.

A rough comparison between the energy spectra shown in Figure 1 does not indicate that most of the measured neutrals result from penetration through and reappearance from the surface. That is, the energy loss of $H^0$ and the width of the energy spectrum of $H^0$ are not very different from those of the $H^+$ ions. In order to compare the energy spectra in detail, the energy losses of the $H^+$ ions and neutrals are shown in Figure 2 at 0.4 MeV incidence. The energy losses of the neutrals were almost equal to those of the $H^+$ ions. This shows that the ratio of reflected ions at the topmost layer of the surface among the measured neutrals is almost the same as that for $H^+$ , since the energy-loss collisions along the ions trajectories are expected to be almost the same regardless of their final charge states. The enhancement of neutral fractions by the penetrated ions appears in the low-energy tail of the spectra. The tail of neutrals was slightly larger than that for $H^+$, as can be seen in Figure 1. However, the contribution of the small yield of the tail is not significant.

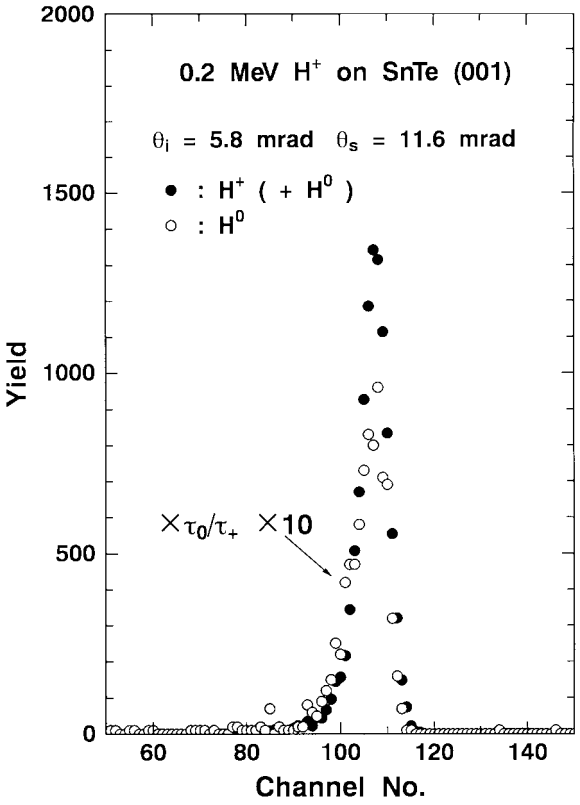


**Fig. 1.** Examples of the energy spectra of scattered ions at 0.2 MeV $H^+$ ion incidence with $\theta_i = 5.8$ mrad. Open circles are for $H^0$ and closed circles are for $H^+$, where $H^0$ ions are also detected and contribute 0.5% of the yield. The measuring time for $H^0$ is $\tau_0/\tau_+ = 14.6$ times larger than that of $H^+$ and the yield of $H^0$ is multiplied by 10.

Examples of the $\theta_s$-dependence of the neutral fraction are shown in Figure 3 at 0.2 MeV incidence. The angles for specular reflection ($\theta_s = 2\theta_i$) corresponding to the angles of incidence are shown by arrows. The neutral fractions show a dependence for the angles: the fractions increase steeply as the angle of scattering decreases at $\theta_s \leqq 2\theta_i$, and they increase slightly as the angle of scattering increases at $\theta_s \geqq 2\theta_i$. The dependence is different from that of the ratio of the charge state fraction $He^+/He^{2+}$ discussed in [5,14].

The incidence energy dependence of the neutral fraction was measured at the angle for specular reflection with $\theta_i = 4.4 \pm 0.1$ mrad. The measured fractions are shown in Figure 4 by closed circles. The fractions decrease as the energy of incidence increases. The order of the neutral fractions (less than 1%) agrees with that measured at Al(111) and Si(111) surfaces [8,15].

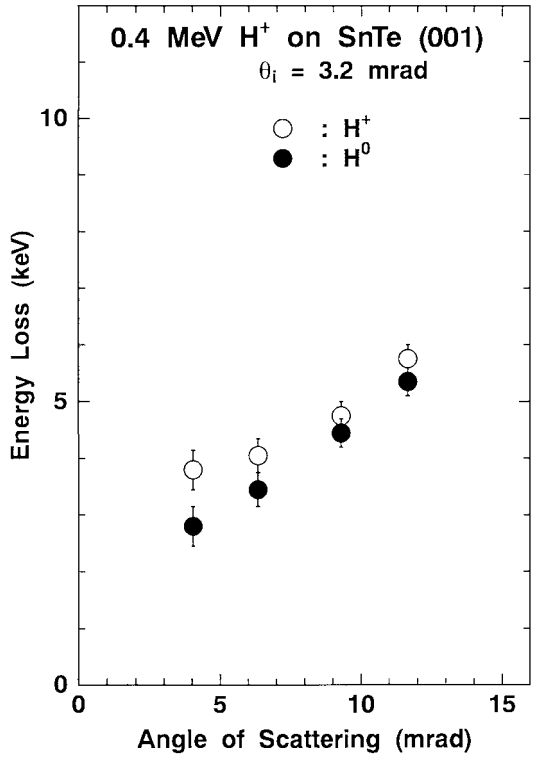


**Fig. 2.** Examples of the scattering angle dependence of the energy loss of $H^+$ and $H^0$ ions at the incidence of 0.4 MeV $H^+$ ion with $\theta_i = 3.2$ mrad.

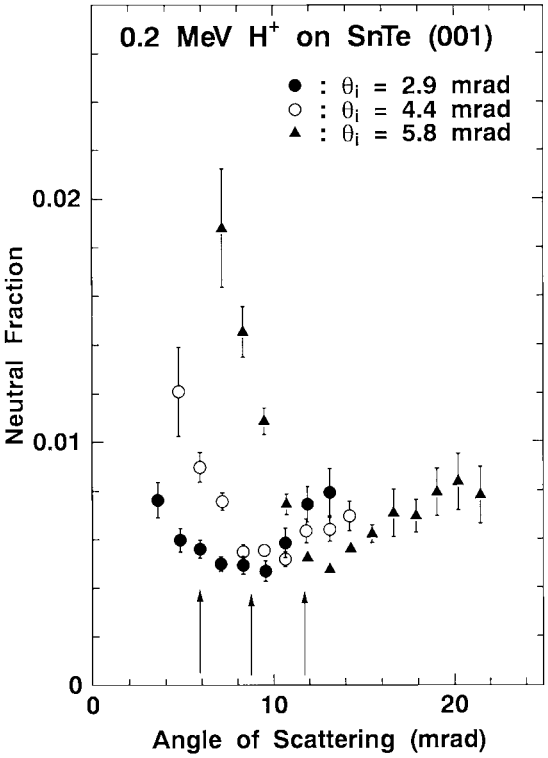


**Fig. 3.** Scattering angle dependence of the neutral fraction $\Phi_0$ for 0.2 MeV ions. The angles for specular reflection are indicated by arrows.

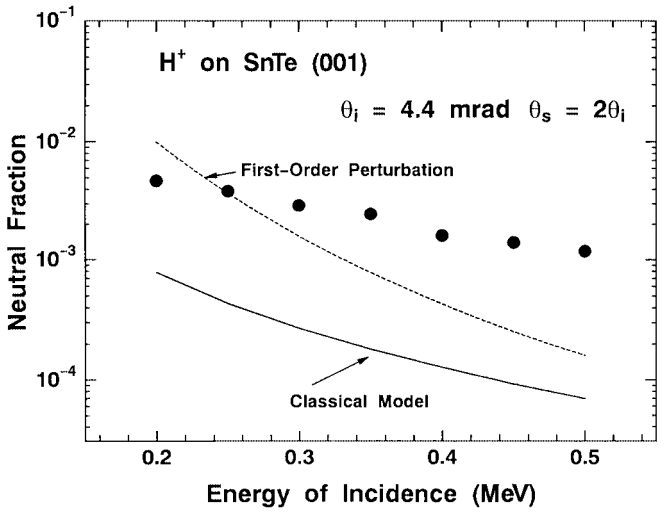


**Fig. 4.** Incidence energy dependence of the neutral fraction $\Phi_0$ measured at $\theta_s = 2\theta_i$ for $\theta_i = 4.4 \pm 0.1$ mrad. The error bars are smaller than the circles. The solid line is the calculated one by using the probabilities $Q_l(z)$ and $Q_c(z)$ obtained by the classical model. The dashed line is that obtained by the first-order perturbation model.

## 3 Calculations of the neutral fraction

The ions reflected on the topmost layer of the surface atomic plane were studied in this work to explain the observed neutral fractions. A Cartesian coordinate frame fixed with respect to the surface of the crystal was considered, where the $xy$-plane is parallel to the surface and the $z$-axis is parallel to the surface normal. The $H^0$ fraction $\Phi_0$ of the ion moving almost parallel to the $x$-axis along the trajectory $z(x)$ is written by

$$\frac{d\Phi_0}{dx} = Q_c(z(x))\Phi_1 - Q_l(z(x))\Phi_0 \,, \qquad (1)$$

where $\Phi_1 = 1 - \Phi_0$ is the fraction of $H^+$ and $Q_c(z(x))$ and $Q_l(z(x))$ are the probabilities for electron capture and electron loss per unit path length along $x$, respectively. The fraction $\Phi_0$ was calculated by equation (1), using the trajectories $z(x)$ of the specular reflection of $H^+$ ions under the surface continuum potential derived from the Molière approximation for the Thomas-Fermi-type screening function. The initial condition was $\Phi_0 = 0$, *i.e.*, $H^+$ ion incidence. The fraction of $H^-$ was neglected.

Two types of theoretical models were used to calculate $Q_c(z(x))$ and $Q_l(z(x))$. One is based on the classical Bohr and Bohr-Lindhard models [1], and the other is based on the first-order perturbation theory [16]. Since the details of the classical model have been reported in [5,14] and those of the first-order perturbation theory are in [16], only relevant points are mentioned in the following. Auger processes for electron loss and capture were neglected here, since the projectile velocity is larger than $2.5v_0$ [8,17].

### 3.1 Classical model

The Bohr and Bohr-Lindhard models were improved by Fujii *et al.* [14] to calculate the probabilities of charge exchange which depend on the distance from the atomic plane.

The probability for electron loss is calculated by

$$Q_{\rm l}(z) = Q_{\rm ln}(z) + Q_{\rm le}(z)\,, \tag{2}$$

which is the sum of the contribution of collisions with a screened target nucleus, $Q_{\rm ln}(z)$, and of collisions with target electrons, $Q_{\rm le}(z)$. The distribution function obtained by the $H^0$ $1s$ wavefunction was used to distribute the projectile electron around the projectile nucleus. The contribution $Q_{\rm ln}(z)$ was calculated assuming that the electron loss of the projectile occurs when the projectile electron approaches the nucleus within the distance, where the transferred energy in the collision is equal to the binding energy of the projectile electron. The potential of the target nucleus was approximated by the screened Coulomb potential. The contribution $Q_{\rm le}(z)$ was calculated only for the electrons of the target atom whose velocities were smaller than the projectile velocity. The electron loss of the projectile occurs when the transferred energy in the collision is equal to the binding energy of the projectile electron. The distribution of electrons, which depends on the distance from the surface, was approximated by summing the distributions of electrons of the isolated atoms on the surface.

Figure 5(a) shows the calculated probabilities for electron loss of 0.2 MeV $H^0$ on the SnTe(001) surface. The probability for collisions with target electrons, $Q_{\rm le}(z)$, is separated by two contributions: that of the inner-shell electrons of the target atoms, $Q^{\rm i}_{\rm le}(z)$, and that of the outermost electrons ($5s$ and $5p$ electrons of Sn and Te atoms), $Q^{\rm o}_{\rm le}(z)$. That is

$$Q_{\rm le}(z) = Q^{\rm i}_{\rm le}(z) + Q^{\rm o}_{\rm le}(z)\,. \tag{3}$$

Thus the total electron loss probability $Q_{\rm l}(z)$, shown by a solid line in the figure, is given by a sum of three contributions, $Q_{\rm ln}(z)$, $Q^{\rm i}_{\rm le}(z)$ and $Q^{\rm o}_{\rm le}(z)$. The most part (83%) of the total electron loss probability was due to collisions with the target nucleus and with the inner-shell electrons. However, the probabilities $Q_{\rm ln}(z)$ and $Q^{\rm i}_{\rm le}(z)$ decreased more steeply compared with $Q^{\rm o}_{\rm le}(z)$ as the distance from the surface increase. At a distance larger than 2 Å, electron loss was dominated by collisions with the outermost electrons.

For calculating the electron capture, the distribution of electrons of the target atom on the surface was approximated by that of the isolated atoms and was integrated to a function of the distance from the atomic row of the target. The electron capture probability was calculated as an impact-parameter-dependent function. By integrating the results on the surface of the crystal along the $y$-axis, the electron capture probability, which depends on the distance from the surface, was obtained as

$$Q_{\rm c}(z) = Q^{\rm i}_{\rm c}(z) + Q^{\rm o}_{\rm c}(z)\,, \tag{4}$$

where $Q^{\rm i}_{\rm c}(z)$ is the sum of the contributions of the inner-shell electrons and $Q^{\rm o}_{\rm c}(z)$ is the sum of the contributions of the outermost electrons.

Figure 5(b) shows the calculated probabilities for electron capture of 0.2 MeV $H^+$ in collisions with inner-shell electrons, $Q^{\rm i}_{\rm c}(z)$, and the outermost electrons, $Q^{\rm o}_{\rm c}(z)$, on the SnTe(001) surface. The total electron capture probability $Q_{\rm c}(z)$ is shown by the solid line. The most part (96%) of total electron capture probability was due to the collisions with the inner-shell electrons. (The contribution was largest for N-shell electrons of Sn and Te atoms for this incidence energy.) However, the probability $Q^{\rm i}_{\rm c}(z)$ decreased more steeply than $Q^{\rm o}_{\rm c}(z)$ as the distance from the surface increased. At distances larger than 1.5 Å, electron capture was dominated by the collisions with the outermost electrons. Comparisons between Figure 5 (a) and (b) show that the probability for electron capture decreased more steeply than that for electron loss. Thus the position-dependent neutral fraction, $Q_{\rm c}(z)/(Q_{\rm l}(z) + Q_{\rm c}(z))$, decreased as the ions left the surface in outward trajectories.

### 3.2 The first-order perturbation model

The first-order perturbation model used here is based on that by Kaneko *et al.* [16], which was proposed for the calculation of neutral fractions of MeV ions penetrating a single crystal under channeling conditions. The calculation has given results which agree with experimental data for protons incidence at energies larger than 0.5 MeV on Ni low-indices planar channels [16]. The incident energy, $E_{\rm i}$, required for this model in the present system ($H^+$ on SnTe crystal) is $E_{\rm i} \gg 70$ keV.

For the electron loss probability, only the contribution due to the collisions with screened target nucleus was considered. The initial state of a transferred electron was the $H^0$ $1s$ state and the final state is the plane wave. The screened Coulomb potential is used for the potential of the nucleus of the target atom.

For the electron capture probability, the wavefunctions of target atom electrons were approximated to be $H^0$ $1s$ like the one with screening parameters obtained by their binding energies. The initial state of the transferred electron was an approximated state of the target atom and the final state was $H^0$ $1s$. The screened Coulomb potential was used for the potential of the nucleus of the target atom.

The probabilities $Q_{\rm l}(z)$ and $Q_{\rm c}(z)$ of this model were also expressed as functions of the distance from the surface atomic plane. The main information from the result was almost the same as that for the classical model, *i.e.* the probability for electron capture decreased more steeply than that for electron loss as the distance from the surface increased.

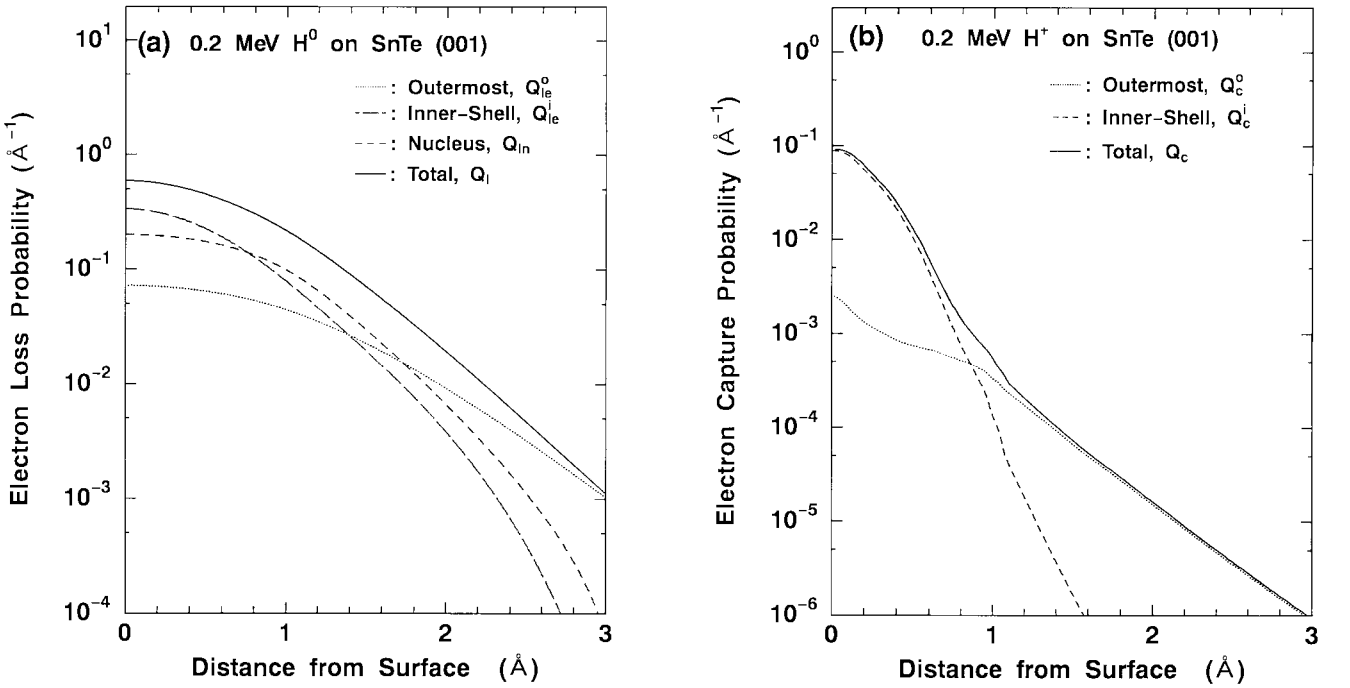


**Fig. 5.** Calculated electron loss and capture probabilities obtained by the classical model. (a) Electron loss probabilities of 0.2 MeV $H^0$. The dotted line shows the probabilities in collisions with the outermost electrons ($5s$ and $5p$ electrons) of the target atoms. The long-dashed line shows those with inner-shell electrons. The short-dashed line shows those with the target nucleus. The solid line shows the total electron loss probability $Q_l(z)$. (b) Electron capture probabilities of 0.2 MeV $H^+$. The dotted line shows the probabilities for the outermost electrons of the target atoms. The dashed line shows those for the inner-shell electrons of the target atoms. The solid line shows the total electron capture probability $Q_c(z)$.

## 4 Discussion

### 4.1 Comparison between the experimental and calculated results

The neutral fraction $\Phi_0$, calculated by solving equation (1) for trajectories $z(x)$ with the probabilities obtained by the classical model, is shown in Figure 4 by a solid line. The calculated result was about one order of magnitude smaller than the experimental ones. This disagreement contradicts the facts that the cross-sections calculated with the classical models expressed the charge states of ions passing through gaseous and solid targets very well [18–24], and that the charge state fractions of $He^+$ and $He^{2+}$ reflected from the (001) surface of SnTe at glancing-angle scattering are also expressed very well by the classical model [5,14].

The calculated results of the first-order perturbation model are shown in Figure 4 by a broken line. The line decreases steeper than the experimental one as the energy of incidence increases. Although this agrees with experimental results of energy of incidence lower than 0.3 MeV, it becomes smaller as the energy of incidence increases. The probability of the electron loss treated in the present model does not include the contribution of collisions with target atom electrons. Further, the energy of incidence required for calculation with this model must be larger than 70 keV. The calculated results using an energy of incidence less than 0.3 MeV may be inadequate. A similar situation can be seen in [8] for the Al (111) surface.

Although the valence electrons contributed only slightly to the total probabilities of electron loss and capture, they were dominant for charge exchanges at distances from the surface, $z$, larger than 1.5 Å. In the present calculations the role of valence electrons on the final charge states of ions were very important, because the charge state fractions change along their outward trajectories at 1.5 Å $< z <$ 2 Å due to the large electron loss probability of $H^0$. This situation is different from that of scattering $He^+$ on the same surface, where the charge state fraction grows at the distance $z <$ 1.3 Å. Thus the final fraction of $He^+$ is influenced more by the capture of N-shell electrons from the target atoms [5,14].

Both models treated above approximated the states of electrons on the surface by averaging those of the isolated atoms arranged regularly on the planar lattice. However, the states of valence electrons of the target atoms change drastically from isolated atoms when they bond together and form a solid. The states of valence electrons at a surface of solid are different from those of electrons in the solid and their energy distribution is localized at several eV below the Fermi energy of the solid [25–28]. The disagreements between the experimental and calculated results are expected to result from collisions with the valence electrons at the surface.

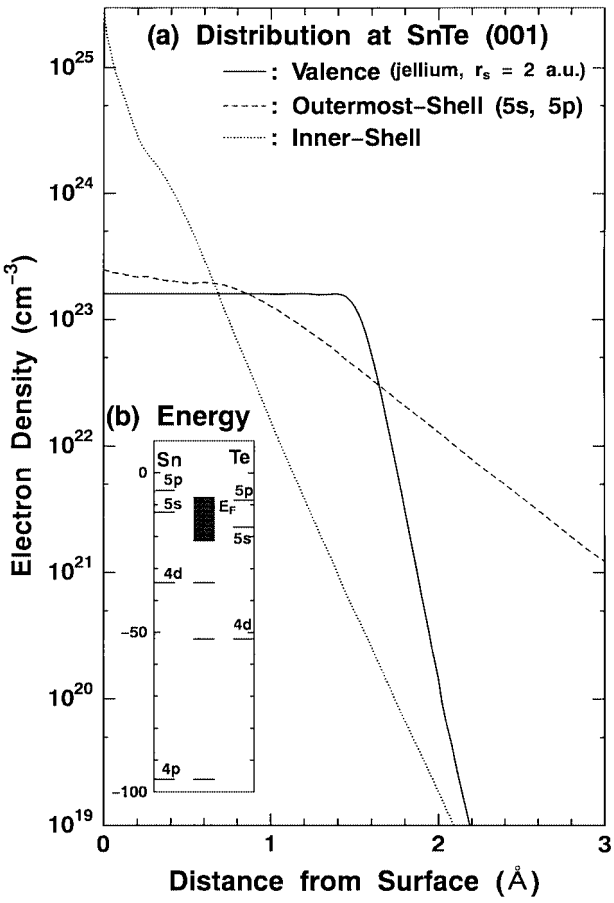


**Fig. 6.** (a) Electron distribution at the (001) surface of SnTe. The solid line shows the valence electron density where the jellium background model ($r_s = 2$) is assumed. The dotted line shows the density of the inner-shell electrons and the dashed line shows that of the outermost electrons ($5s$ and $5p$ electrons of Sn and Te atoms). (b) Binding energies (in eV) of electrons for Sn and Te atoms are shown on the left and right sides. The Fermi energy of SnTe, $E_F$, is also shown in the middle. The hatched area shows the energies for valence electrons on the surface.

### 4.2 Electron capture cross-section of $H^+$ ions in collisions with valence electrons at the surface

Theories of the distributions and density of states on the surface have yet to be fully realized [25–28]. In studies on charge exchanges in the keV energy region, valence electrons are treated as free electrons [29]. This treatment is also used for calculating the energy loss of projectiles at the glancing-angle incidence of MeV ions [10,13,30]. The electron distribution calculated in the jellium background positive charges has been frequently used [6,7]. The one-electron radius, $r_s$, for SnTe is 2.17 a.u., which is obtained from the density of valence electrons, $n = 2.35 \times 10^{-2}$ a.u. The electron distribution $n_v(z)$ for $r_s = 2$ a.u. is compared with that of the averaged outermost-shell electrons of the atom in Figure 6(a) [7]. The surface of the positive background is assumed to be at $d_p/2$, where $d_p = 3.16$ Å is the interplanar distance of the SnTe crystal. The distribution for the jellium background model concentrates compared with that of the outermost electrons of the isolated atoms. In order to clarify the present model system, the energies of valence electrons at the surface were shown by comparing the Fermi energy in Figure 6(b) with the energy of the electrons in isolated atoms.

In order to obtain the electron capture cross-sections of $H^+$ in collisions with valence electrons at the surface, the neutral fraction $\Phi_0$ was calculated as follows.

For electron loss due to collisions with the target nucleus and inner-shell electrons, the probabilities were obtained by the classical Bohr model. The probability for an electron loss due to collisions with valence electrons was achieved by multiplying the distribution for valence electrons by an adjustable parameter $\sigma_l^v$, which is the cross-section of electron loss of $H^0$ in collisions with valence electrons. Thus the total probability for the electron loss $Q_l(z)$ is given by

$$Q_l(z) = Q_{ln}(z) + Q_{le}^i(z) + \sigma_l^v n_v(z)\,. \tag{5}$$

For electron capture due to collisions with the inner-shell electrons of the target atoms, the probability was obtained by the classical Bohr-Lindhard model. Similarly, the total probability for the electron capture $Q_c(z)$ is given by

$$Q_c(z) = Q_c^i(z) + \sigma_c^v n_v(z)\,, \tag{6}$$

where $\sigma_c^v$ is an adjustable parameter that is the cross-section of electron capture of $H^+$ in collisions with valence electrons.

The pair of the cross-sections $\sigma_l^v$ and $\sigma_c^v$ was searched to final value where the neutral fraction $\Phi_0$ calculated by equation (1) agrees with the experimental one. An example of the results is shown in Figure 7 by solid lines for the 0.2 MeV incidence. The circle in the figure shows the values for a single electron calculated by the classical model for the outermost ($5s$ and $5p$) electrons of Sn and Te atoms.

For the electron loss cross-sections $\sigma_l^v$, those measured at the electron impact on $H^0$ with collision velocities equal to those of the present experiment were chosen [31]. The electron capture cross-sections $\sigma_c^v$ could then be obtained by Figure 7. The results of the cross-sections are shown in Figure 8. Possible errors were estimated by errors of $\Phi_0$ and $\sigma_l^v$, and those due to the use of the classical model, which were estimated by adjusting $Q_c^i(z)/(Q_{ln}(z)+Q_{le}^i(z))$ within a factor 2, because the model reproduces many experimental data within a range of factors [18–24]. The errors due to the assumed distribution of valence electrons were also estimated by adjusting the position of the surface of the positive background by 10%. The later errors were dominant and shown in the figure for 0.2 and 0.5 MeV. For comparison, the cross-sections of a single electron obtained by the classical model for the outermost electrons are shown in the figure.

The electron loss cross-sections agree with those obtained by the classical model. However, the electron capture cross-sections are 3-20 times larger than those obtained by the classical model. The dependence on the

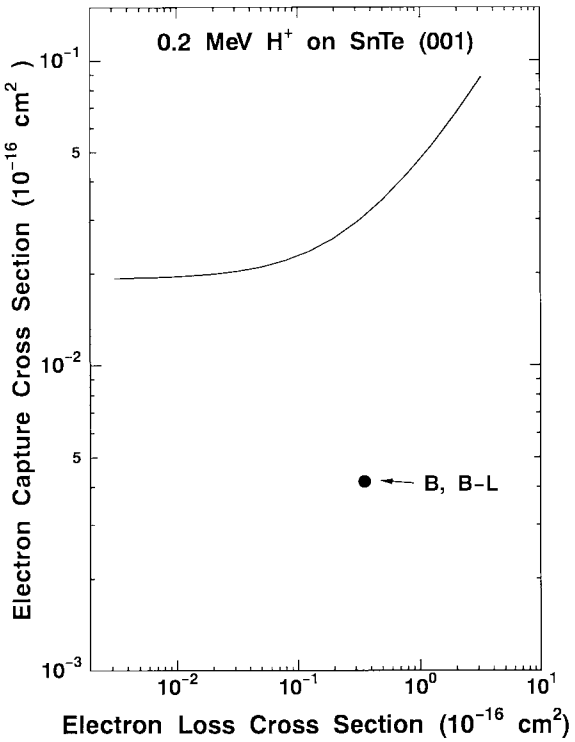


**Fig. 7.** Electron capture cross-section of 0.2 MeV $H^+$ *versus* electron loss cross-section of $H^0$ in collisions with valence electrons at the (001) surface of SnTe to reproduce the experimental neutral function. The closed circles show the cross-section for a single electron obtained by the classical model.

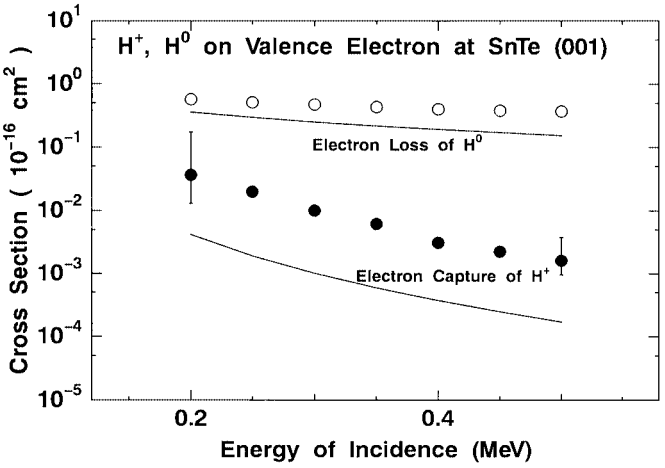


**Fig. 8.** Electron capture cross-sections of $H^+$ for valence electrons at the (001) surface of SnTe. Electron loss cross-sections of $H^0$ in collision with valence electrons are also shown, which are the electron impact ionization cross-section of $H^0$ measured with the equal collision velocity taken from [31]. The typical errors are shown at 0.2 and 0.5 MeV, which were estimated by the error due to the assumed distribution of valence electrons. The cross-sections obtained by the classical model are shown by solid lines.

energy of incidence agrees well with that calculated by Bohr-Lindhard model. Thumm and Briggs proposed a model of proton neutralization at the surface, where the Thomas-scattering process is said to be dominant [32]. The probability for neutralization was treated in the second-order Born approximation on a broken line trajectory of protons in their work. Since they wished to emphasize the physical effects of interaction, their calculations did not include the electron loss of $H^0$ resulting from neutralization, which is important for the calculation of neutral fractions on the outward trajectory. Their calculated results overestimate the experimental ones [8]. Presently, however, no work other than the processes of neutralization pointed out in their work followed by the electron loss is available to explain the present disagreement between the experimental and calculated results.

A model has been proposed for the dependence of the charge state fractions on the angle of scattering at the glancing-angle incidence of MeV $He^+$ ions taking the atomic steps at the surface into consideration [5]. In this model, the trajectories of the ions scattered at angles smaller than that for specular reflection, $\theta_s < 2\theta_i$, are terminated suddenly by the down step of atomic height during the growth of the charge state of ions. Thus the $\theta_s$-dependence of the charge state fraction at $\theta_s < 2\theta_i$ could be estimated using the calculated fraction as a function of distance from the surface. The experimental results for 0.2 MeV ions show that the neutral fraction increases as the angle of scattering decreases within $\theta_s < 2\theta_i$. The dependence can be explained by the present model, where the neutral fraction changes at the outward trajectory from a few percents at $z = 1.5$ Å to the experimental one at $z > 2.5$ Å. When the outward trajectory of the ions is terminated and the ions appear at angle $\theta_s < 2\theta_i$, the neutral fraction is large compared with that of the specularly reflected ions. This is consistent with the observed scattering-angle dependence of the neutral fraction shown in Figure 3.

## 5 Conclusion

The neutral fractions of specularly reflected beams measured at a glancing-angle incidence of (0.2–0.5) MeV $H^+$ ions on a clean surface have been compared with the calculated results based on two models, where the electronic states of valence electrons at the surface are approximated by those of the outermost electrons of the isolated atoms. They differ greatly due to collisions with valence electrons at the surface. Because of the large electron loss probability of $H^0$, the neutral fraction of the specularly reflected beams is almost completely determined by electron capture at large distances from the surface, $z > 1.5$ Å. The electron capture cross-sections of (0.2–0.5) MeV $H^+$ ions for valence electrons at the surface have been derived from the measured neutral fractions. The obtained electron capture cross-sections are about ten times larger than those for the outermost electrons calculated by the classical model.

This experiment was performed while the author was a scientific associate in the Department of Engineering Science, Kyoto University. The author acknowledges Mr. H. Mukai, Mr. T. Baba and Mr. S. Fukui for their help in the experiment. The author is grateful to the members of the Department of Nuclear Engineering of Kyoto University for the use of the 4 MV Van de Graaff accelerator. The author is indebted to Professor M. Mannami and Professor K. Kimura for the use of their experimental apparatus.

## References

1. N. Bohr, K. dan Vidensk, Selsk. Mat. Phys Medd. **18**, No. 8 (1948); N. Bohr, J. Lindhard, K. dan Vidensk, Selsk. Mat. Phys. Medd. **28**, No. 7 (1954).
2. S. Shakeshaft, L. Spruch, Rev. Mod. Phys. **51**, 369 (1979).
3. R.A. Mapleton, *Theory of charge exchange*, in *Wiley-Interscience Series in Atomic and Molecular Collisional Process*, edited by C.F. Barnett (John Wiley & Sons Inc., New York, 1972).
4. K. Kimura, M. Hasegawa, Y. Fujii, M. Suzuki, Y. Susuki, M. Mannami, Nucl. Inst. Meth. Phys. Res. B **33**, 358 (1988).
5. Y. Fujii, S. Fujiwara, K. Kimura, M. Mannami, Nucl. Inst. Meth. Phys. Res. B **58**, 18 (1991).
6. W. Kohn, L.J. Sham, Phys. Rev. **140**, A1133 (1965).
7. N.D. Lang, W. Kohn, Phys. Rev. B **1**, 4555 (1970).
8. H. Winter, R. Kirsch, J.C. Poizat, J. Remillieux, Phys. Rev. A **43**, 1660 (1991).
9. M. Mannami, K. Kimura, K. Nakanishi, A. Nishimura, Nucl. Inst. Meth. Phys. Rev. B **13**, 587 (1986); K. Kimura, H. Ohtuka, K. Ohsima, M. Mannami, Nucl. Inst. Meth. Phys. Rev. B **90**, 227 (1994).
10. K. Kimura, M. Hasegawa, M. Mannami, Phys. Rev. B **36**, 7 (1987).
11. Y. Susuki, T. Ito, K. Kimura, M. Mannami, J. Phys. Soc. Jpn **61**, 3535 (1992).
12. Y. Susuki, H. Mukai, K. Kimura, M. Mannami, J. Phys. Soc. Jpn **59**, 1211 (1990).
13. K. Narumi, Y. Fujii, K. Kishine, H. Kurakake, K. Kimura, M. Mannami, Surf. Sci. **293**, 152 (1993).
14. Y. Fujii, K. Sueoka, K. Kimura, M. Mannami, J. Phys. Soc. Jpn **58**, 2758 (1989).
15. H. Winter, J.C. Poizat, J. Remillieux, Nucl. Inst. Meth. Phys. Res. B **67**, 345 (1992).
16. T. Kaneko, Y.H. Ohtsuki, M. Kitagawa, Rad. Eff. **54**, 183 (1981).
17. R. Zimny, Z.L. Mišković, N.N. Nedeljković, Lj.D., Nedeljković, Surf. Sci **255**, 135 (1991).
18. S. Kreussler, R. Sizmann, Phys. Rev. B **26**, 520 (1982).
19. I. Ben Itzhak, A. Mann, M. Meron, B. Rosner, Phys. Rev. A **40**, 2928 (1989).
20. Y. Haruyama, K. Kanamori, T. Kido, A. Itoh, F. Fukuzawa, J. Phys. B **16**, 1225 (1983).
21. A. Itoh, M. Asari, F. Fukuzawa, J. Phys. Soc. Jpn **48**, 943 (1980).
22. C.F. Barnett, H.K. Reynolds, Phys. Rev. **109**, 355 (1958).
23. N. Cue, N.V. CastroFaria, M.J. Gaillard, J.C. Poizat, J. Remillieux, Nucl. Inst. Meth. **170**, 67 (1980).
24. A. Chateau Thierry, A. Gladieux, B. Delaunay, Nucl. Inst. Meth. **132**, 553 (1976).
25. J.R. Smith, J.G. Gay, F.J. Arlinghaus, Phys. Rev. B **21**, 2201 (1980).
26. M. Posternak, H. Krakauer, A.G. Freeman, D.D. Koelling, Phys. Rev. B **21**, 5601 (1980).
27. S.L. Tang, R.V. Kasowski, A. Suna, B.A. Parkinson, Surf. Sci. **238**, 280 (1990).
28. L.N. Kantorovich, J.M. Holender, M.J. Gillan, Surf. Sci. **343**, 221 (1995).
29. M. Kato, Y.H. Ohtsuki, Nucl. Inst. Meth. Phys. Res. B **135**, 324 (1998).
30. Y. Susuki, Phys. Rev. A **56**, 2918 (1997).
31. W.L. Fite, R.T. Brackmann, Phys. Rev. **112**, 1141 (1958).
32. U. Thumm, J.S. Briggs, Nucl. Inst. Meth. Phys. Res. B **43**, 471 (1989).